Géotechnique

Centrifuge modelling of root-soil interaction of laterally-loaded trees under different loading conditions

GEOT-2021-088-R1 | Paper

Submitted on: 19-08-2021

Submitted by: Xingyu Zhang, Jonathan Knappett, Anthony Leung, Matteo Ciantia, Teng Liang, Bruce Nicoll

Keywords: CENTRIFUGE MODELLING, PARTIAL SATURATION, SOIL-STRUCTURE INTERACTION, SUCTION, VEGETATION

Centrifuge modelling of root-soil interaction of laterally loaded trees under different loading conditions

Zhang, X.[1], Knappett, J.A.[1*], Leung, A.K.[2], Ciantia, M.O.[1], Liang, T.[3], Nicoll, B.C.[4]

[1]University of Dundee, Dundee, UK.

[2]Hong Kong University of Science and Technology, Hong Kong SAR; Formerly University of Dundee, Dundee, UK.

[3]Center for Hypergravity Experimental and Interdisciplinary Research, Zhejiang University, Hangzhou, China; Formerly University of Dundee, Dundee, UK.

[4]Forest Research, Northern Research Station, Roslin, UK.

Original submission:

Keywords: centrifuge modelling, partial saturation, soil/structure interaction, suction, vegetation

No. of words: 7530

No: of tables: 7

No. of figures: 16

*Corresponding author: Professor J. A. Knappett

School of Science and Engineering

University of Dundee

Dundee

DD1 4HN

T: +44-1382-384345

F: +44-1382-344816

E:j.a.knappett@dundee.ac.uk

Centrifuge modelling of root-soil interaction of laterally loaded trees under different loading conditions

Xingyu Zhang, Jonathan Knappett, Anthony Leung, Matteo Ciantia, Teng Liang, Bruce Nicoll

ABSTRACT

Understanding the stability of trees under lateral loads arising from natural hazards (e.g. extreme weather and debris flows) is important as fallen trees can become a potential threat to life and infrastructure. Two 1:20 scale 3D printed analogue root system models with architectures from field-surveyed root architecture data, were used to simulate the push-over behaviour of trees in silty sand under different conditions in the centrifuge. The peak overturning moments obtained were verified against data from field winching tests. Horizontal roots orientated in the loading direction and the central taproot complex contributed most to the overturning resistance. Increasing soil matric suction due to a lowering of the water table, increasing the loading rate and considering the presence of the fine root fraction all resulted in higher moment capacity and rotational stiffness of the root systems. The overturning behaviour was ductile in fully saturated soil and more brittle in partially saturated cases, with more root breakages in the windward horizontal roots and the taproot complex in the latter. These results suggest that it is important to measure the groundwater conditions when conducting winching tests and demonstrate a connection between soil effective stress, total root breakage area and peak moment resistance.

KEYWORDS: centrifuge modelling, partial saturation, soil/structure interaction, suction, vegetation

INTRODUCTION

Landslides and debris flows, which are common natural hazards in alpine regions (Lateltin *et al.*, 2005), can cause ecosystem degradation and vegetation destruction (Cui *et al*., 2012). An upward trend in windstorms (Schelhaas *et al*., 2010) is also a major hazard that causes damage in European forests (Gandhi *et al*., 2008; McCarthy *et al*., 2010). Given that landslides and debris flows generate monotonic lateral loading at the bottom of tree trunks and windstorms induce cyclic lateral loading along tree trunks, the behaviour of trees under lateral loads, including understanding tree-root-soil interaction has therefore been of significant interest in forestry e.g. tree resistance to windthrow (Stokes, 1999; Mickovski & Ennos, 2003; Nicoll *et al*., 2008), to inform forest management plans to cope with wind risks (Gardiner & Quine, 2000; Dupont & Brunet, 2008; Moore *et al.*, 2008). Understanding the mechanisms of soil-root interaction is also of interest in civil engineering, as windthrow of trees may be a potential threat to life and infrastructure (Schmidlin, 2009) and in sloping ground may become a trigger for landslides (Nelson *et al.*, 2015; Jakob & Lambert, 2009).

The pushover stability of a tree has been investigated chiefly through a combination of field winching tests (Coutts, 1983; Crook & Ennos, 1996, 1998; Nicoll *et al.*, 2006a) with analyses of strain around the base of the trunk, root system architecture measurement (Danjon *et al.*, 2005, 2008; Nicoll *et al*., 2006b), and mechanical tests on individual roots (Schwarz *et al.*, 2011). However, in the field, it is impossible to find identical root system architectures to enable a systematic study of variables and the variation in water and soil conditions along the rooting depth is difficult to detect.

To address this issue, reduced-scale 1$\boldsymbol{g}$ physical modelling studies in the lab (Zhang *et al.*, 2018; Harnas *et al.*, 2016; Mickovski *et al.*, 2010) have previously been con-

ducted to enhance the understanding of root-soil interaction. However, only highly simplified roots/root systems, which did not fully capture root architecture, were employed and these physical models may underestimate the push-over resistance as branching pattern has been shown in separate studies to have a large effect on root-soil interactions (Mickovski *et al.*, 2007; Meijer *et al.*, 2019). Additionally, the confining stresses in such 1***g*** models did not represent field conditions (confining stress around 10 kPa) due to the reduced depths of the root analogues in the models.

To overcome these difficulties, Zhang *et al.* (2020) recently developed repeatable 1:20 scale models of full tree root architectures using 3D printing based on field measurement data to validate 1***g*** scaling laws related to fully drained tree-pushover behaviour. However, because of the limited resolution of the 3D printer, the fine (non-structural) roots were omitted during the construction of the scaled models. Little is known about how this affects the mechanical interaction. In addition, considering the horizontal loading from natural hazards (e.g. wind, rockfall, landslides), the shearing rate in reality may be significantly faster than drained laboratory tests or typical field winching tests, potentially inducing positive/negative excess pore water pressure and/or soil suction change due to the rapid root-soil relative movement, which may affect the root-soil interaction and overturning behaviour. Mickovski *et al.* (2010) and Kamchoom *et al.* (2014) found the presence of soil suction enhanced the root-soil interaction significantly, and Kamchoom *et al.* (2014) attributed this to increased tendency of constraint dilatancy upon soil-root interface shearing, while Défossez *et al*. (2021) showed that the moment resistance of laterally loaded trees in sandy soil did not decrease drastically with soil wetting until the soil was fully saturated. These findings suggest that more research is required to understand the potential differences between field winching tests potentially conducted in drier ‘summer’ soil conditions and critical loading conditions

after heavy rainfall. Some numerical studies on root-soil interaction of trees under lateral loads (e.g. Rahardjo et al., 2009; Yang *et al*., 2017; Kim *et al*., 2020; Ramos-Rivera *et al*., 2020) have suggested that rooting length and depth and windward roots contributed mostly to the tree anchorage strength. However, how these findings on root-soil interaction mechanics translate to different loading conditions (groundwater, rate) is uncertain. Therefore, further study is required to consider these variables.

This paper employs the scaled models developed in Zhang *et al.* (2020) to conduct an extensive series of physical push-over tests at 20***g*** in a geotechnical beam centrifuge to study the failure mechanisms and moment-rotation relationships of contrasting root systems as affected by: (i) fine (non-structural) roots; (ii) rate of loading; (iii) soil saturation conditions (by adjusting the groundwater table level); and (iv) root system architecture.

CENTRIFUGE MODELLING

Soil type and properties

The model soil used in this study was a mixture of 70% HST95 silica sand and 30% A50 non-plastic silt, which attempted to simulate key mechanical properties of a field sandy loam (known as Bullionfield soil, see Liang *et al*., 2017; Meijer *et al*., 2018) in terms of particle size distribution (PSD, Fig. 1(a)) and shear strength (Fig 1(b)), but which could be air-pluviated around a 3D printed root model of complex geometry. The laser diffraction method (BS1377: 1990 Part 1) was employed to determine the PSD of the model soil and the coefficients of uniformity and curvature of the model soil were found to be 15.1 and 2.4, respectively. A further PSD curve for a sandy spodosol representing the soil at the locations of the trees whose root architectures were used for the 3D printed root models is also shown. Other basic index properties are summarised in

Table 1. A series of saturated drained direct shear apparatus (DSA) tests using a standard 60 mm × 60 mm × 50 mm split box were conducted to determine the shear strength properties of the soil at an air-pluviated relative density of 45-50% (representative of later centrifuge models). The critical-state friction angle of the model soil was 37.8°, which is close to that of saturated compacted Bullionfield soil (36.4°), previously tested under similar direct shear conditions (Liang *et al*., 2017). In this study, the partially saturated shear strength of the non-plastic model soil may be estimated by the following effective stress equation proposed by Khalili & Khabbaz (1998):

$$\tau = c' + [(\sigma - u_a) + \chi(u_a - u_w)]\tan\phi' \quad (1)$$

where c' is cohesion (0 for the model soil), σ is total normal stress, u_a is pore air pressure (atmospheric), u_w is pore water pressure, ϕ' is friction angle, and χ may be defined as $(s/s_e)^{0.55}$ (where s and s_e are matric suction (i.e. $(u_a - u_w)$) and air-entry value, respectively).

Drying and wetting soil water retention curves (SWRCs, Fig. 2) were determined using five replicates sieved in 100 cm^3 steel rings with the same relative density as the DSA tests. Each sample was subjected to suctions ranging from 1 to 1500 kPa using a tension table (1–50 kPa; Soilmoisture Equipment Corp, USA) and a pressure plate apparatus (50–1500 kPa; Soilmoisture Equipment Corp, USA). The SWRC was fitted by the van Genuchten model (van Genuchten, 1980) in terms of volumetric water contents:

$$\theta_w = \theta_r + \frac{\theta_s - \theta_r}{[1+|\alpha\psi|^n]^m} \quad (2)$$

where θ_w is the soil water content (cm^3/cm^3), θ_r and θ_s are the residual and saturated soil water contents, respectively, ψ is soil matric suction (kPa), and α, n and m $(m = (1 - 1/n))$ are model parameters. Each sample was first dried from the fully saturated condition to a matric suction of 1500 kPa, followed by a wetting path to 0.1 kPa. The test results, as well as the fitting parameters for the van Genuchten model,

125 depicted in Fig. 2 show that the air-entry value of the model soil is approximately 2
126 kPa, which is similar to that of Bullionfield soil (3 kPa, *Liang et al*., 2017). Marked
127 hydraulic hysteresis was observed after experiencing a cycle of drying and wetting.
128

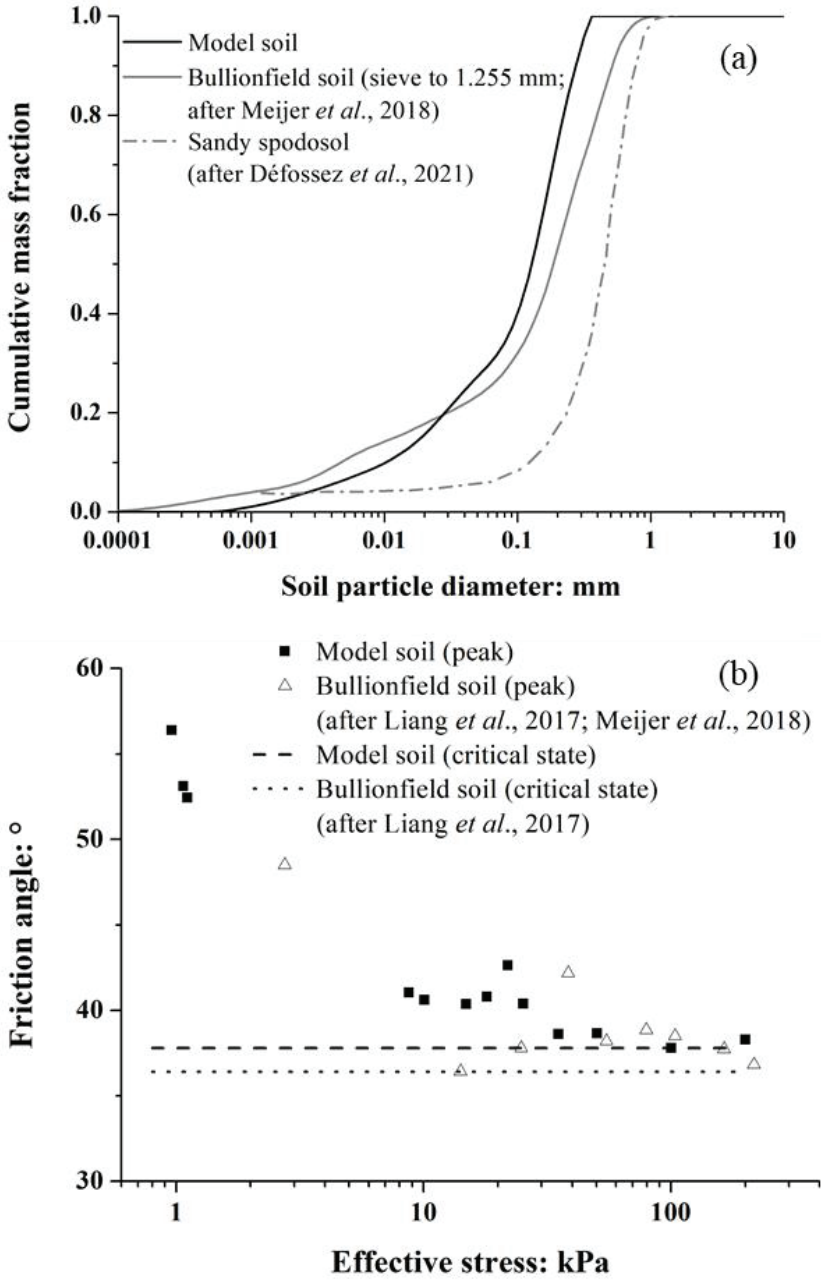

129

130 **Fig. 1. Comparison of the properties between the model soil and Bullionfield soil: (a) particle**
131 **size distribution; (b) friction angle**

132 **Table 1. Index properties of model soil**

Soil	Value	Units
Specific gravity	2.65	-
Maximum density	1.9	Mg/m^3
Minimum density	1.5	Mg/m^3
Maximum void ratio	0.77	-
Minimum void ratio	0.4	-
D_{10}	0.01	mm
D_{30}	0.06	mm
D_{50}	0.12	mm
D_{60}	0.16	mm
Coefficient of uniformity	15.1	-
Coefficient of curvature	2.4	-

133

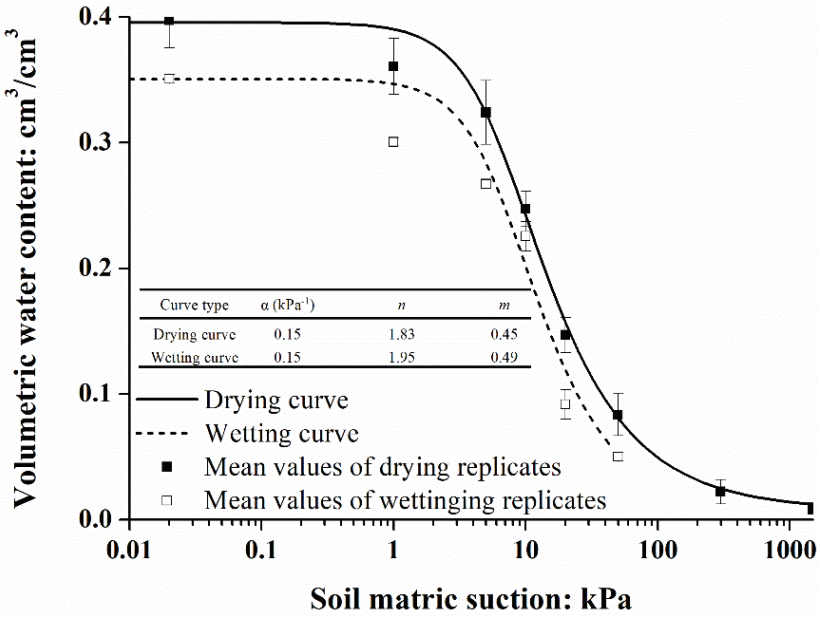

134

135 **Fig. 2. Model soil water retention curve of soil sieved to relative density of 48%; mean values**

136 **of replicates (±Standard error) are used in curve fitting for the van Genuchten (1980) model**

137

138 *3D printed root system*

139 Two 1:20 geometrically scaled 3D root models with distinctively different, yet realistic,

140 architectures were reconstructed digitally and 3D printed in this study. The first model

141 had a relatively narrow and deep architecture (ND), whereas the other was wider and

142 shallower (WS). The ND model was created from root architecture data reported from
143 a 27-year-old *Pinus pinaster* tree grown in a deep sandy spodosol, which is similar to
144 the soil used in this study, in the "Landes de Gascogne" forest in south-west France
145 (Fig. 3(a), after Danjon & Reubens, 2008). The WS model was from a 19-year-old *P.*
146 *pinaster* tree also grown in a shallower sandy spodosol in Cestas, France (Fig. 3(b),
147 after Danjon *et al*., 2013). Some traits of the two root models are summarised in Table
148 2. In this study, the central taproot is considered as the first-order root. This first-order
149 root branched hierarchically into second-order roots and so on. The resolution of the
150 3D printer used limited the smallest root that could be printed to a diameter of 1.6 mm
151 at model scale (32 mm at prototype scale). In this case, four types of rods with a uniform
152 diameter of 1.6, 2, 2.4 and 3 mm (model scale) and tortuosity matching the field meas-
153 urements were used to simulate the structural roots, while the diameter of the taproot
154 varied along its length according to the field survey. To compensate for the loss of fine
155 root material due to the limited resolution of the 3D printer, the total root volume of the
156 models was scaled-up to match the volume of the real root systems as outlined in Zhang
157 *et al.* (2020).
158
159 **Table 2. Dimensions of roots at prototype**

Root systems	Spread of lateral root* (m)	Root depth* (m)	Root volume (cm^3)
ND	2.4	1.8	103270
WS	3.0	1.3	169100

*Spread of lateral root: maximum distance from stem centre to lateral root
*Root depth: maximum distance from stem centre to tap root

160
161 To quantify root morphology, the rooted area was divided into eight zones relative
162 to the prevailing wind direction (marked on Fig. 3) as presented in Fig. 4. For simplified
163 expression, zones VIII and I are defined as 'windward', zones II, III, VI and VII as
164 'side', and zones IV and V as 'leeward' zones. For both models, apart from the taproot

complex, more than 75% of the total number of roots originated within the top 20 mm of the ground surface at model scale (0.4 m at prototype scale), and only these roots are shown for comparison. Fig. 4 shows that although the WS model has more roots in total than the ND model, the latter had one more lateral in zone V, forming a symmetric structure in the leeward zones, with the same number of horizontal roots in the windward zones as the WS model.

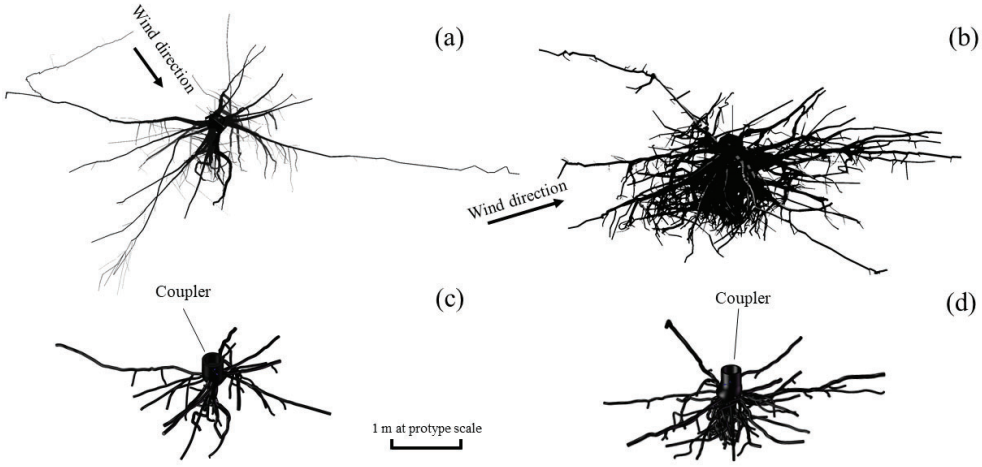

Fig. 3. Reconstruction of roots from field measured data and simplified models for printing: (a) (c) Narrow and deep (ND) system; (b) (d) Wide and shallow (WS) system (wind direction is marked by the arrows)

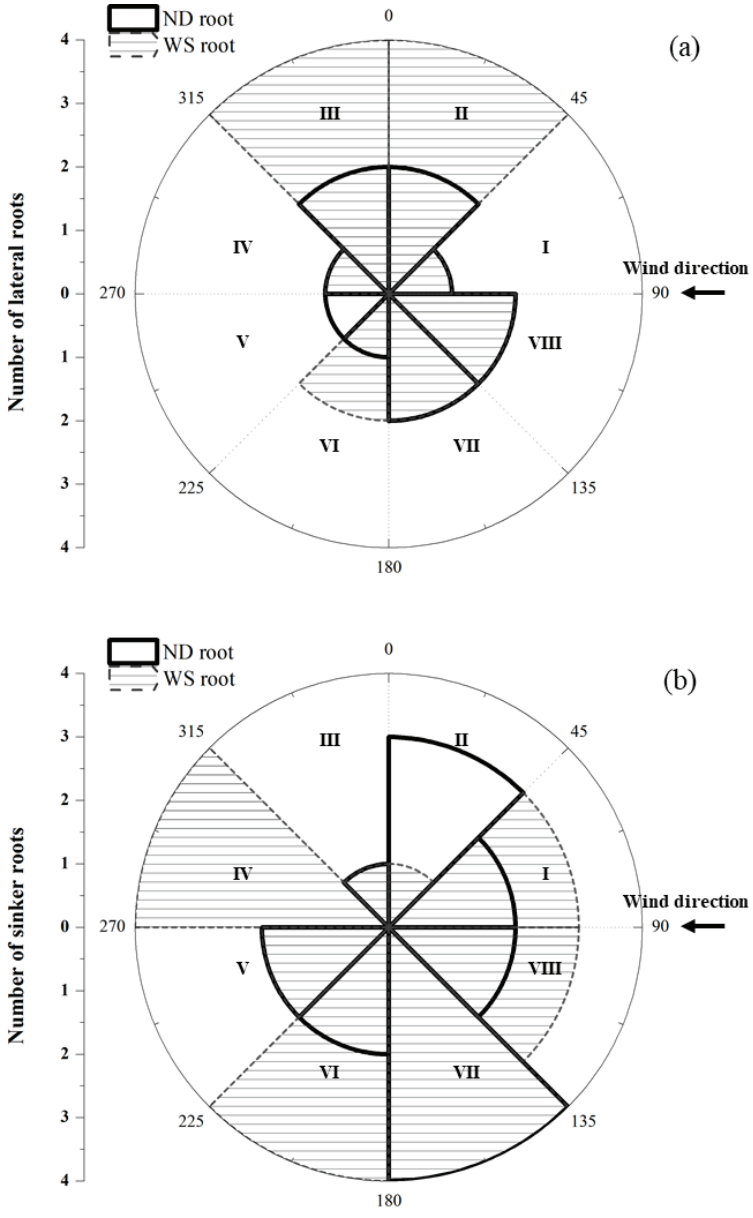

176

177 **Fig. 4. Number of (a) lateral and (b) sinker roots of ND and WS models in different zones**

178 **(plan view)**

179

180 Root models were printed using a Fortus 250mc 3D printer using Acrylonitrile Bu-

181 tadiene Styrene (ABS) plastic, which has previously been demonstrated to have me-

182 chanical properties highly representative of tree roots (in terms of tensile strength,

183 Young's modulus and brittle breakage at failure) through a series of uniaxial tension

and bending tests (Liang *et al.*, 2015) across a range of model root diameters. The interface properties of this material have been investigated in Liang *et al.* (2020). The mean particle size (D_{50}) of the soil used was 0.12 mm, while the weighted average diameter of the 3D printed root model was 2 mm. This means that the ratio of D_{50} to weighted average root diameter is 17. This ratio is larger than the threshold of 15, beyond which any particle size effects can be effectively ignored (Stone &Wood, 1992).

A 14 mm diameter pine wood dowel connected with a coupler to the root system was used to model the tree trunk to provide a relatively rigid lever arm (Zhang *et al.*, 2018) for applying horizontal load and converting this into an overturning moment on the root system. Following Défossez *et al*. (2021), the canopy was not considered in this study. This additionally avoids any parasitic loading on the model from the airflow within the centrifuge chamber.

Table 3. Scaling laws used in this study (after Wood, 2004, Nakahara *et al*., 2005)

Parameter	Scaling law: Model/Prototype
Length/Depth	$1/N$
Mass density	1
Acceleration	N
Stiffness	1
Stress	1
Force	$1/N^2$
Displacement	$1/N$
Pore fluid viscosity	1
Time (diffusion)	$1/N^2$
Velocity	N
Moment	$1/N^3$
Rotation angle	1

Test program, setup and procedures

Ten centrifuge tree push-over tests were performed using the Actidyn C67-2 geotechnical beam centrifuge at the University of Dundee, UK. The scaling laws used in this

study are summarised in Table 3, while the test programme is outlined in Table 4. From this point onward, all dimensions are expressed at prototype scale, unless stated otherwise. Three tests were conducted for the ND models. Tests XZ02 and XZ03 aimed to study the root anchorage behaviour in the model soil with different groundwater levels, one at the ground surface and one at 1.85 m depth (hence the entire root system was within the partially saturated zone), under an identical push-over rate. Given the weighted-average prototype root diameter $d_{r,ave}$ of 40 mm, the coefficient of consolidation C_v of the model soil of 2.6 mm^2/s (measured from oedometer tests), and the non-dimensional Peclet number, defined as

$$Pe = \frac{v d_{r,ave}}{C_v} \quad (3)$$

(Finnie & Randolph, 1994), the maximum rate of shearing v of soil to ensure drained shearing behaviour should not exceed 3.9 mm/min, for a Peclet number smaller than the threshold value of 1. Therefore, the model rate of 0.03 mm/min adopted in this study is considered suitable to achieve drained root-soil interaction everywhere within the root system in the fully saturated case (Test XZ02). Test XZ10 also considered the ND model but was tested at a much faster rate of 180 mm/min (or 0.003 m/s), which approaches the typical range of loading rate for landslides (Table 5, after Meijer *et al*., 2015). The WS root system was also tested across a similar range of saturation conditions and loading rates (Tests XZ07 to XZ09). In tests XZ09 and XZ10, the Peclet number in the soil at 300 mm (prototype scale) away from the root system centre (approximately 1/10 of the spread of the lateral roots and considering the root system to rotate as a rigid body about the base of the trunk) was higher than 10, which is representative of undrained shearing behaviour, while soil very close to the central roots (within 300 mm at prototype scale) was in the transition zone between drained and undrained conditions.

Table 4. Centrifuge test programme (water table and loading rate are presented at prototype scale)

Test Number	Root model	Nominal water table	*g*-level	Loading rate
XZ02	ND	saturated	20	0.03 mm/min
XZ03	ND	1.85 m depth	20	0.03 mm/min
XZ04	ND + fibres	saturated	20	0.03 mm/min
XZ05	ND + fibres	1.85 m depth	20	0.03 mm/min
XZ06	ND + fibres	1.05 m depth	20	0.03 mm/min
XZ07	WS	saturated	20	0.03 mm/min
XZ08	WS	1.85 m depth	20	0.03 mm/min
XZ09	WS	saturated	20	180 mm/min
XZ10	ND	saturated	20	180 mm/min

Table 5. Typical shear rates for landslides, debris flows, field shear box testing, and lab shear box testing presented at prototype scale (after Meijer *et al.*, 2015)

Loading type	Loading rate: m/s
Debris flow	4.9×10^{-1} - 1.8×10^{1}
Landslide	1.0×10^{-3} - 1.0×10^{1}
Shear box (field)	2.5×10^{-5} - 3.2×10^{-4}
Shear box (lab)	1.6×10^{-6} - 5.0×10^{-5}

Tests XZ04 to XZ06 investigated the effect of fine root material on the push-over behaviour. Flexible crimped polypropylene fibres, Loksand^{TM}, with a nominal length of 35mm, a nominal diameter of 0.1mm, a specific gravity of 0.91 and a tensile strength of 200MPa (Wang & Brennan, 2015), were added (unconnected) around the 3D printed ND system, such that the total root volume (fibres/fine roots + printed roots) was equivalent to that of the WS system. The fibres were unconnected from the printed roots as it was infeasible to connect these to the printed roots with representative mechanical properties. Use of fibres therefore does not incorporate the direct structural effects of fine root material on push-over behaviour, but attempts to capture the indirect effect of this material on the response of the larger structural roots. In this way, comparison with the ND tests (XZ02 and XZ03) shows the influence of discarding fine root material too

small to be printed (or the effect of only accounting for the larger structural roots in the modelling assumptions), while comparison with the WS tests (XZ07 and XZ08) permits study of root systems of similar total volume, but with either only part of this formed by structural roots (ND + fibres) or with it all formed from such roots (WS). Effects of different groundwater conditions were also investigated, including fully saturated conditions and two different lowered water table depths at 1.05 and 1.85 m below ground level (BGL).

For the push-over tests conducted at the slower rate of 0.03 mm/min, a strongbox container with internal dimensions of 16 m × 10 m × 11 m (at prototype scale) was used. At the bottom of the container, a 0.6 m thick pea-gravel layer was placed to facilitate saturation. This was overlain by a 2 m thick HST95 pure sand layer with a relative density of 50-60% and then subsequently by a 6 m thick layer of the model soil (Fig. 5(a)). Two 1:20 scale root models were installed within each soil bed, since the plan area of the container was large enough to test two root models (offset either side of the container centreline) without interfering with each other (Fig. 5(b)). Each root model was suspended at the desired position and the model soil was pluviated around them through a 1.18 mm sieve at a fixed height of 450 mm (at model scale) from the soil surface to create a uniform 6 m thick layer of model soil with an average relative density of 45-50% (corresponding to a dry bulk density of 1.67±0.02g/cm^3, close to 1.58g/cm^3, the average value of the field soil measured at 0.4-0.6 m depth (prototype scale) in Défossez *et al*. (2021)). Pluviation was complete when the soil surface reached the underside of the coupler. In the fully saturated tests the container was saturated bottom-up using water under a water head 500 mm (at model scale) higher than the soil surface. For partially saturated tests, an external standpipe with drainage holes at different vertical positions was connected to the bottom of the container and hung from it to set a

target elevation for the water table. These models were initially fully saturated with all standpipe holes blocked; an overflow was subsequently installed at the appropriate elevation in the standpipe before the sample was left to equilibrate.

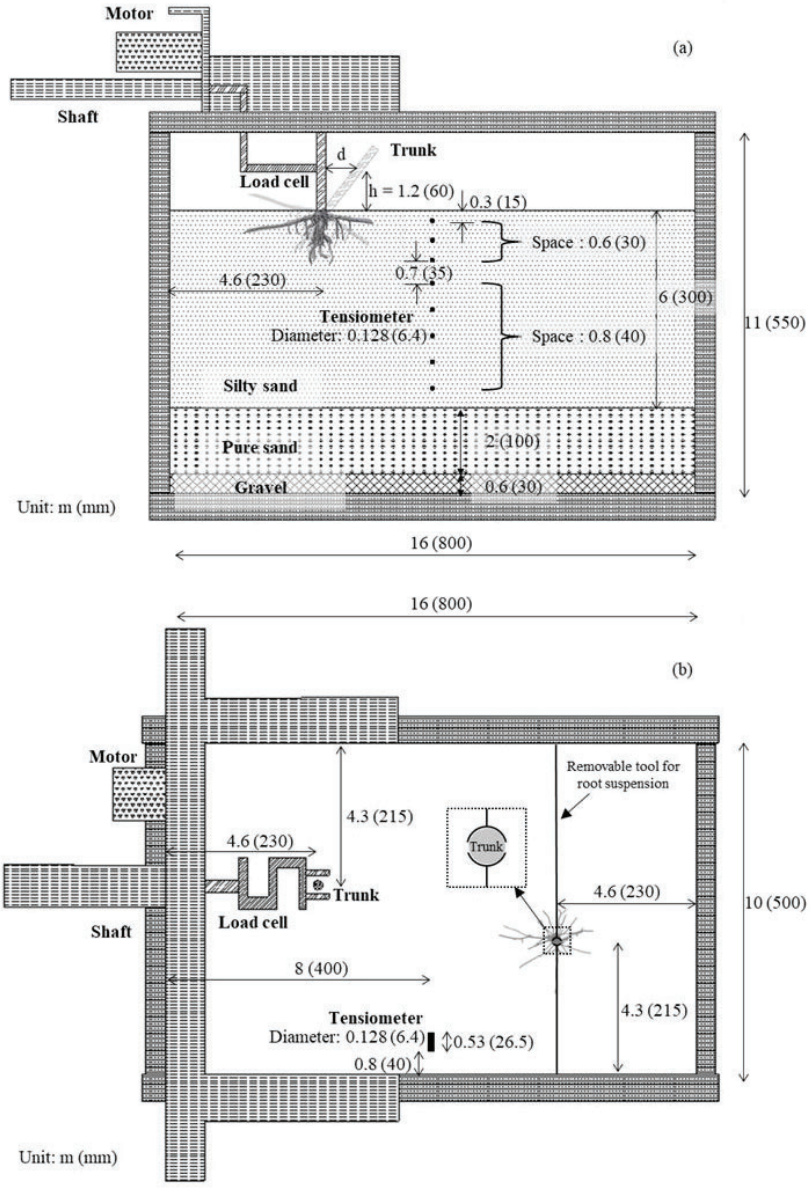

Fig. 5. Diagram of test set-up for centrifuge tests: (a) elevation view; (b) plan view (dimensions at prototype scale, with model dimensions expressed in the brackets)

276 A vertical array of eight EPB-PW-7BS tensiometers (each with a 1-bar ceramic po-
277 rous stone; StrainSense Ltd, UK), spaced between 0.6 – 0.8 m, was installed in the soil
278 to measure the pore water pressure distribution with depth (Fig. 5(a)). As shown in Fig.
279 6, the pore water pressures at equilibrium at the test ***g***-level were distributed hydrostat-
280 ically with depth. The maximum matric suction found at the soil surface was approxi-
281 mately 10 and 18 kPa for the case of 1.05 and 1.85 m depth of the water table, respec-
282 tively. According to the soil water retention curve shown in Fig. 2, these suction values
283 mean that the model roots were tested within the so-called "transition zone" of the
284 curve, where the role of suction on soil shear strength would be prominent.
285

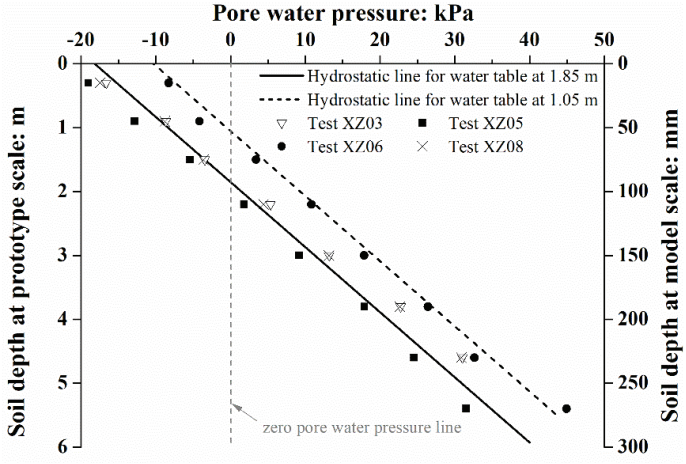

286

287 **Fig. 6. Pore water pressure along the soil depth for four partially saturated tests at prototype**
288 **scale**

289

290 For the tests that considered the effects of fine roots, two layers of fibres (3.74 g in
291 each layer) were distributed uniformly around the top and bottom of the ND root system,
292 covering approximately 0.2 m^2 rooted area at prototype scale.

293 After spinning the centrifuge to the target ***g***-level (20***g***) and ensuring that the tensi-
294 ometers had reached equilibrium, a displacement-controlled lateral action was applied

295 to the trunk at 1.2 m above the top of the coupler (Fig. 5(a)) in order to induce an
296 overturning moment onto the model root system. This position maximised the rotation
297 angle achievable (approximately 30°) for the given travel of the actuator. The loading
298 was applied in the direction of the prevailing wind as indicated on Fig. 3. Moment-
299 rotation ($M-\theta$) curves were determined from the measurements of loading time (t)
300 and loading rate (v_H) to obtain displacement, with lateral force (F) obtained using a
301 200 N tension load cell (model RLT, RDP Electronics Ltd, UK), via:

302 $$\theta = \tan^{-1}\left(\frac{tv_H}{h}\right) \quad (4)$$

303 $$M = Fh + 0.5m_tNghLsin(\theta) \quad (5)$$

304 where h was the distance between the loading point and the top of root (Fig. 5(b)), m_t
305 and L were the mass and the length of the trunk, respectively, N was the $\boldsymbol{g}$-level and $\boldsymbol{g}$
306 gravitational acceleration. The second term in Equation (5) accounts for the weight of
307 the trunk, given θ was large.

308 For Tests XZ09 and XZ10 at a much faster loading rate of 180 mm/min (also under
309 displacement control), an Actidyn in-flight loading system (IFLS) P67-2L was used
310 due to its ability to rapidly translate in the horizontal direction. The model preparation
311 procedures of these two tests were identical to those described above, but using a
312 strongbox of a larger plan area and reduced height (18 m × 13 m × 9 m at prototype
313 scale) consistent with the footprint of the IFLS. In these tests, the actuator travel was
314 greater; after pushing the trunk to 50° rotation (denoted as step one), the actuator was
315 reversed by 1.2 m (pulling it out of contact with the trunk), followed by a second push
316 at the same rate but to a further 30° rotation (step two). These additional loading stages
317 (i.e. step two), performed immediately following step one without stopping the centri-
318 fuge, aimed to study the residual capacity of a rotated tree, such as might occur when
319 subject to multiple landslide events.

It should be noted that the response of the ABS plastic is reproducible following Liang *et al*. (2015) and that the relative density of the model soil was verified by using six density cups to ensure its reproducibility (Fig. S1, supplementary material). All other key variables (e.g. root architectures, groundwater conditions and loading conditions) were closely controlled in all tests. The results presented in this study consequently have high level of repeatability, where previously-reported tests using the same root model at the same effective stress regime have been demonstrated to give similar results (Fig. S2 & S3; Zhang *et al*., 2020). Further discussion relating to repeatability of the model push-over can be found in the Supplementary Material.

RESULTS

Observed failure patterns of model roots

For each test, the broken roots (complete breakages) recovered from the soil, post-test, are marked in black in Fig. 7. Some broken roots which were still attached (partial breakages) are marked in grey. All tests conducted in fully saturated soil, irrespective of the root architecture, loading rate, or the presence of fibres (i.e. XZ02, XZ04, XZ07, XZ09 and XZ10), showed pull-out of the windward horizontal roots. For the partially saturated tests, all broken roots remained buried in the soil and no individual roots were pulled-out.

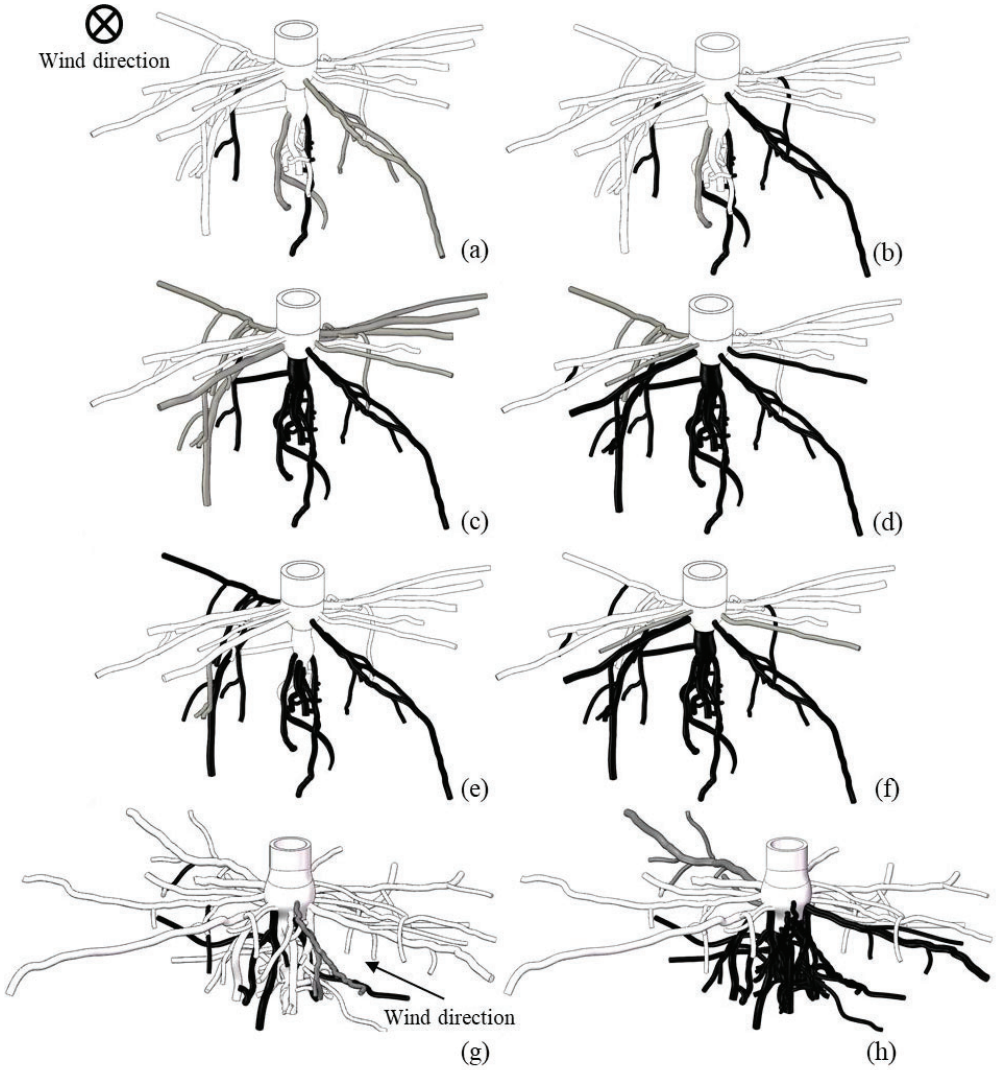

Fig. 7. Broken roots observed in the centrifuge tests: (a) ND in saturated soil (XZ02); (b) ND with fibres in saturated soil (XZ04); (c) ND in partially saturated soil with water table at 1.85 m depth (XZ03); (d) ND with fibres in partially saturated soil with water table at 1.85 m depth (XZ05); (e) ND in saturated soil tested with faster loading rate (XZ10); (f) ND with fibres in partially saturated soil with water table at 1.05 m depth (XZ06); (g) WS in saturated soil (XZ07); (h) WS in partially saturated soil with water table at 1.85 m depth (XZ08)

Effect of soil saturation/position of the water table

Fig. 8(a) compares the moment-rotation curves obtained from ND roots tested in fully saturated and partially saturated soil. For the partially saturated case with the water table

at 1.85 m depth (marginally lower than the lowest part of the ND model – 50 mm at prototype scale), the rotational stiffness was increased by a factor greater than three and the peak moment capacity was approximately twice that in fully saturated soil. If it is assumed that the principle of effective stress applies to describe the strength of the partially saturated soil according to Equation (1), the shear strength at the mid-depth of the root system increased from 8.3 kPa (fully saturated) to 19.5 kPa (partially saturated), an increase by a factor of 2.4 which is similar to the increases in strength and stiffness. Because of this, more root breakages occurred in the partially saturated tests (see Fig. 7(c)), especially on the taproot complex (undamaged in the saturated case; Fig .7(a)) and this was likely responsible for the overall brittle behaviour during overturning. Indeed, while there was only one thinner windward horizontal root broken in the fully saturated soil (Fig. 7(a)), in the partially saturated soil more than 60% of the laterals broke, especially in the windward and leeward directions (Fig. 7(c)). The breakage of the large taproot complex in the partially saturated case was associated with the large reduction in moment at approximately 5° rotation.

Fig. 8(b) shows the effect of three different water table positions for the ND model with fibres (ND + fibres), used to simulate finer roots. A similar change of moment-rotation behaviour from ductile (saturated case) to brittle (partially saturated cases) was observed as for the ND root systems without fibres. Again, the moment capacity and rotational stiffness increased due to the reduction of the water table level consistent with the increase in matric suction. The two partially saturated cases are similar to each other and different to the fully saturated case which appears to agree with previous findings reported by Défossez *et al*. (2021), where root anchorage strength in similar soil did not decrease drastically with soil wetting until the soil reach full saturation. However, this is further explored in the DISCUSSION, below. The overall shapes of

the two curves, as well as the root breakage patterns (Fig. 7(d), (f)), for the lowered water tables were quite similar, both peaking at approximately 6° rotation before a prominent moment drop of 45% to a value similar to the fully saturated case, followed by several sharp yet small magnitude drops at large rotations. Regardless of the existence of fibres, the residual moment resistance of the ND model in partially saturated soil was close to or even lower than that under fully saturated conditions (Fig. 8(a), (b)) because more roots, especially the taproot complex, broke due to the increased effective confining stress.

The WS models in partially saturated soil also displayed a more brittle response, showing higher rotational stiffness, higher moment capacity and more broken roots compared to the fully saturated case (Fig. 8(c)). However, the residual moment of the WS system in partially saturated soil was much higher than that in the fully saturated case, unlike the observations for the ND and ND + fibres cases in Fig. 8(a) and (b). This is discussed further in the root architecture section, below. In the WS model, there were two sharp drops of moment at small rotation angles (approximately 5° and 7.5°; Fig. 8(c)), which were likely associated with the breakage of the main central structural roots as indicated in Fig. 7(h). As internal stresses could be structurally redistributed within the root system, peak moment was finally reached at a rotation of approximately 10°.

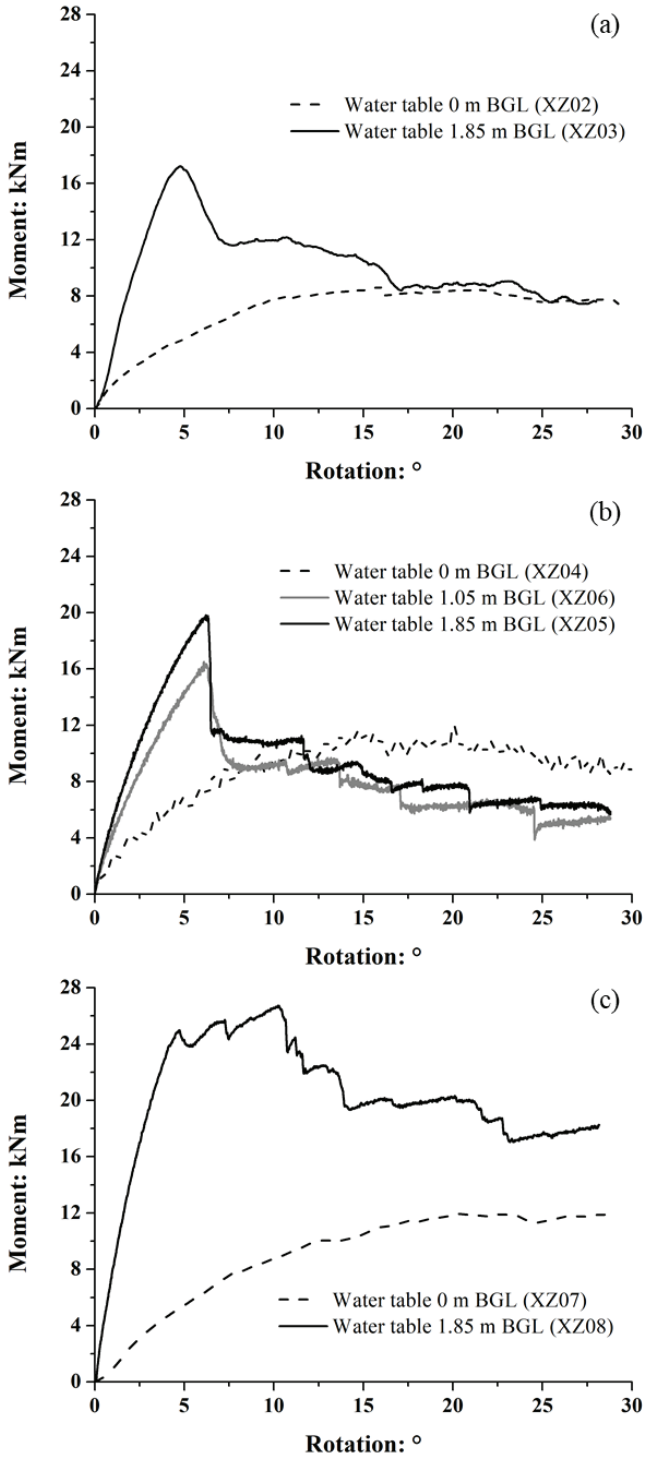

Fig. 8. Comparisons of moment-rotation curves of model tree root systems under different soil saturation conditions: (a) ND model; (b) ND model with fibres (c) WS model (all values expressed at prototype scale)

Effect of neglecting fine root material

Comparisons of the moment-rotation curves depicted in Fig. 9 suggest that the addition of fibres (representing the fine root fraction) did not have a very significant effect on the initial stiffness or ductility of the root system response. The moment capacity did however increase by approximately 20% in both groundwater condition cases, consistent with fibres requiring a significant strain to mobilise their tensile strength and increasing the shear resistance of the soil (e.g. Wang & Brennan, 2015) within which the structural roots are interacting. The breakage patterns of the ND model with or without fine roots in fully saturated soil were almost identical (see Fig. 7 (a), (b)). When the water table was lowered to 1.85 m depth the fibres appeared to protect some leeward laterals from being damaged (Fig. 7(c), (d)). The protected leeward roots may not result in significant increases in resistance at large rotations since they remained attached to the root system (partial breakages) when there were no fibres. It was observed that fibres strengthened the root-soil interaction on the windward side as some failed laterals exhibiting partial breakage without fibres (Fig. 7(c)) became detached (Fig. 7(d)), possibly because the fibres reinforced the soil around the printed roots, contributing additional constraint to (and increasing internal forces within) the printed roots when the relative root-soil displacement was large. This may explain why the residual capacity was lower at 30° rotation in the partially saturated case with the finer roots included (Fig. 9(b)).

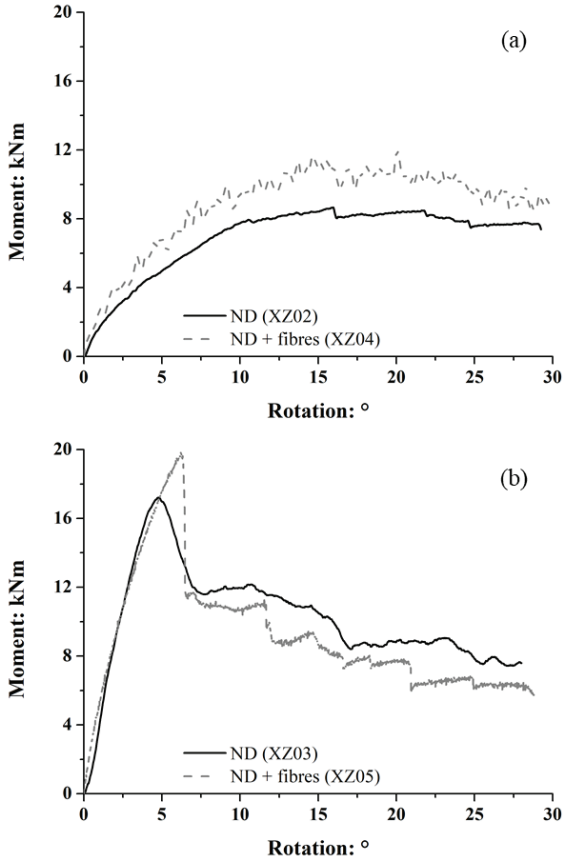

Fig. 9. Effects of including or neglecting fine root material on moment-rotation curves in: (a) fully saturated soil; (b) partially saturated soil with water table 1.85 m (all values at prototype scale)

Effect of loading rate

The test results shown in Fig. 10 depict that irrespective of the root architecture, models subjected to a higher loading rate did not exhibit any significant difference in rotational stiffness up to approximately 5° rotation, but beyond this point, a substantial increase in peak moment capacity was observed (by +80% and +50% for the ND and WS models, respectively). Based on the drained direct shear test results shown in Fig. 1(b), the model soil at an effective vertical stress of approximately 9 kPa (i.e., at the mid-depth of root systems) was dilative upon shearing. This might imply that during rapid partially-drained to undrained pushover, negative excess pore-water pressures might have

431 developed within the soil-root matrix and a corresponding increase in effective confin-
432 ing stress might explain the observed higher moment capacities in Fig. 10. It is reason-
433 able to assume that the observed broken roots post-test (Fig. 7(e)) were mostly from the
434 initial loading stage, because in this stage the model trunk had been pushed to a large
435 rotation of 50°. Compared with the breakage pattern for the comparative drained case
436 (Fig. 7(a)), almost all branches of the ND system's taproot broke (Fig. 7(e); the taproot
437 itself was, however, undamaged). Unfortunately, root breakages in test XZ09 were not
438 recorded as the model was accidently disturbed during post-test model deconstruction.
439

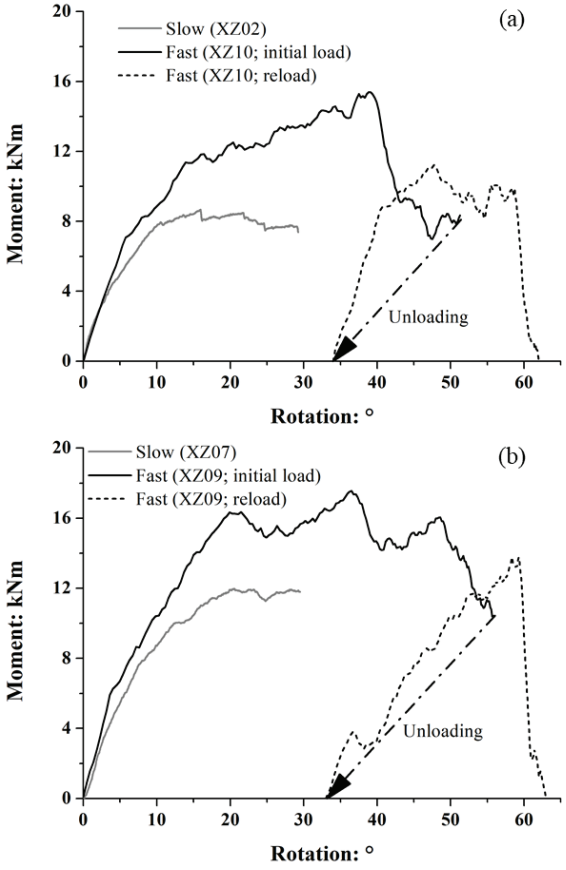

440

441 **Fig. 10. Effects of loading rate on moment-rotation curves of: (a) ND model; (b) WS model**
442 **(all values expressed at prototype scale)**

Upon unloading, the trunk of both models rebounded to approximately 35° rotation. The reloading stage curves in both cases showed that the rotational stiffness was similar to the initial loading stage, and almost 75% of the peak moment capacity from the initial loading stage was preserved as the taproot was still intact. Upon reloading, a significantly more brittle response was identified in both models after the trunk rotated by a further 25° (approximately; 60° in total, accounting for the rebound).

Effect of root architecture

As shown in Fig. 11(a), when tested under fully saturated conditions, the initial rotational stiffness provided by the WS case was similar to that of the ND case, until a rotation of about 5°. By 30° rotation, the peak moment resistance of the WS model was only 35% higher than that of the ND root, even though it had 65% greater total root volume and a wider spread of second-order horizontal roots. This comparatively small difference in moment capacity between these models may be because although the two models had very similar numbers of windward horizontal roots (Fig. 4, zones I and VIII), the stability of trees can be reduced due to an asymmetrical architecture of the shallow roots (e.g. the WS model; Coutts *et al.*, 1999). In addition, the ND root system was 38% deeper than the WS case, meaning that the tap and sinker roots in the ND case could have gained greater resistance from greater effective confining stress for resisting uprooting, offsetting reductions from the main laterals being shorter. By comparing the measurements from the WS model and the ND + fibres model with similar total root volume, the moment-rotation curves were highly similar for the first 15° rotation. At the end of the test, the WS model showed a higher moment capacity. In addition to having a wider spread of horizontal roots, the WS model had a shorter but denser and stiffer central taproot complex, acting like a cage to interact with the surrounding soil. The

468 larger volume of roots branching from the taproot may also have improved the anchor-
469 age by guying the end of the taproot (Danquechin Dorval *et al*., 2016).
470

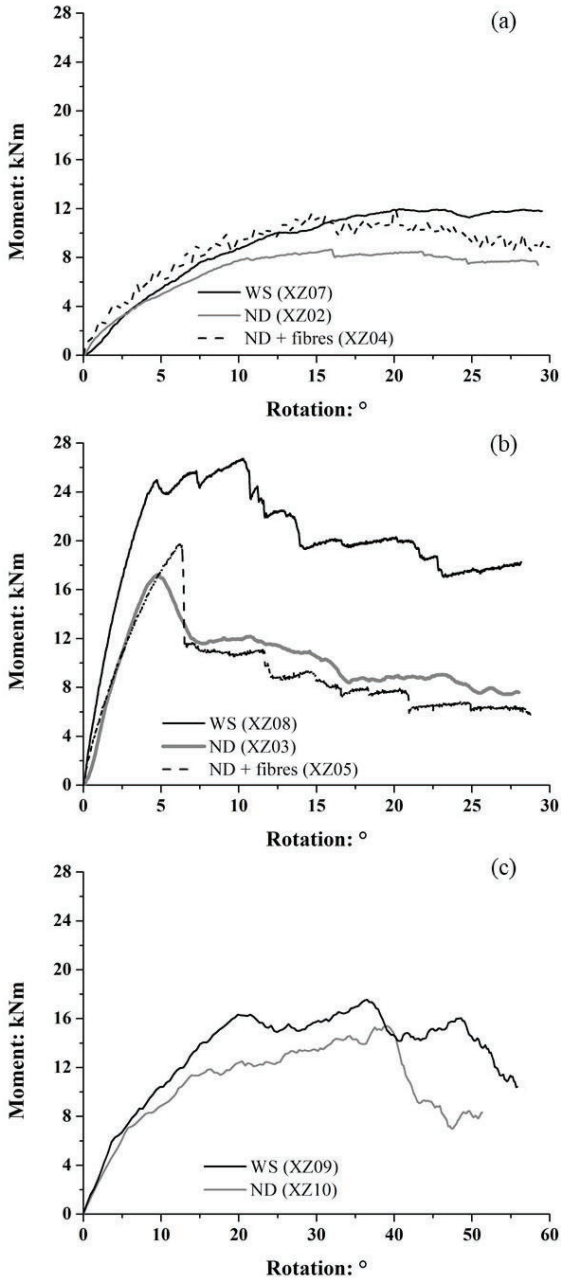

471

472 **Fig. 11. Effects of root architecture on push-over curves under: (a) fully saturated conditions; (b)**
473 **partially saturated conditions with 1.85 m water table; (c) fast loading rate (all values expressed**
474 **at prototype scale)**

When tested in partially saturated soil (Fig. 11(b)), the effects of root architecture on the moment-rotation behaviour were different from those in saturated conditions. While the WS model showed a stiffer and stronger response than the ND model, the moment-rotation curve was less brittle as some breakages of WS roots occurred prior to the peak, resulting in less reduction post-peak. Additionally, the residual capacity of WS was higher than that of ND. This was because the taproot complex of both models broke in the partially saturated soil (Fig. 7(c), (h)), such that the ND system no longer had the advantages of deeper anchorage depth while the WS system retained more widely spread unbroken laterals (Fig. 4) and was therefore less dependent on the taproot complex for its moment capacity. This also explains why when the water table was lowered and the taproot complex was damaged, the WS model exhibited higher residual moment resistance than that in saturated soil (Fig .8c). Despite the same total root volume, the behaviour of the WS and ND + fibres models was different, while the overall responses of ND and ND + fibres models were quite similar, suggesting that the interconnection of the structural roots was more significant than the total root volume in the partially saturated case.

Compared with the fully saturated drained tests (Fig. 11(a)), the difference in peak moment resistance between ND and WS was reduced when tested under a faster loading rate (Fig. 11(c)), in which case the leeward roots were likely mostly mobilised since the models were pushed to a large rotation of 50°. The ND model had one additional leeward horizontal root in zone V (Fig. 4), which could contribute additionally to the moment capacity and offset the difference in the amount of root material (i.e. location, rather than volume is critical).

DISCUSSION

Comparisons with field data from winching tests

Fig. 12 compares the moment-rotation curves between all centrifuge models and *Pinus pinaster* trees tested in the Landes de Gascogne Forest (Nézer forest in the southwest of France), where the field tree used as the basis for the ND was located, reported by Défossez *et al*. (2021). The site was a medium humid sandy spodosol (PSD in Fig. 1(a)) and the topography was flat. The field tests were performed during/after a period of rain with a water table at approximately 0.4-0.6 m depth below the soil surface. In Fig. 12 the curves were normalised by their peak moment (M_p) and the corresponding rotation at the peak moment (θ_p). It was found that the overall shapes of the centrifuge test curves were consistent with the field tests up to the peak. The Défossez *et al*. (2021) field data has a continuous drop of moment post-peak, suggesting few breakages of main structural roots, possibly due to the presence of connected finer roots, or insensitive load measurement.

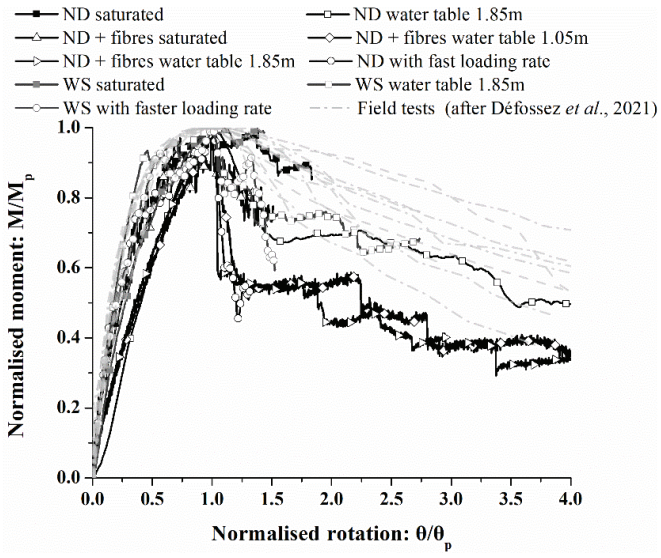

Fig. 12. Comparison of normalised moment-rotation curves with field winching tests in similar soil conditions

From a geotechnical perspective, due to the inclination angle of the winch cable below the horizontal, field winching tests are a combination of horizontal (H), vertical (V) and moment (M) actions on the root system, compared to the push-over tests (H-M) conducted in this study, which aimed to simulate lateral actions from wind and other natural hazards. Using a traditional macroelement approach adapted from shallow foundations proposed by Dattola *et al*. (2020), the influence of the vertical load component V on expected moment capacity was quantified. The moment capacity was defined from the equation of the yield surface by:

$$\frac{M}{D_{eq}V_c} = \eta\sqrt{\xi^2(1-\xi)^{2\beta} - \left(\frac{H}{\mu V_c}\right)^2} \quad (6)$$

where normalised vertical load

$$\xi = \frac{\frac{V}{V_c} - \left(\frac{V_t}{V_c}\right)}{1-\left(\frac{V_t}{V_c}\right)} \quad (7)$$

From Dattola et al. (2020), the empirical parameters controlling the shape of the yield surface η = 3, β = 0.95, μ = 150 and ratio of tensile (uplift) to compressive (bearing) capacity V_t/V_c = -0.12 were calibrated based on 1***g*** tests of the ND root system and D_{eq} (equivalent diameter of the model root system) was taken as 1.06 m based on scaling the 1***g*** calibrated value to prototype scale. For a winching test pulling at angle θ_F below the horizontal using a cable of length L:

$$\frac{H}{\mu V_c} = \frac{1}{\mu\, tan\theta_F}\left(\frac{V}{V_c}\right) \quad (8)$$

Fig. 13 shows the resulting normalised V-M yield surface for L = 1.6 m (mid-point of the 1.4-1.8 m range in the field testing conducted by Défossez *et al*., 2021) and $\theta_F = 24^\circ$ (average value in Nicoll *et al*., 2006a). The load path under centrifuge conditions is vertical in Fig. 13 (V/V_c = 0), while the load path in a winching test is:

$$\frac{M}{D_{eq}V_c} = \frac{L\, cos\theta_F}{D_{eq}}\left(\frac{V}{V_c}\right) \quad (9)$$

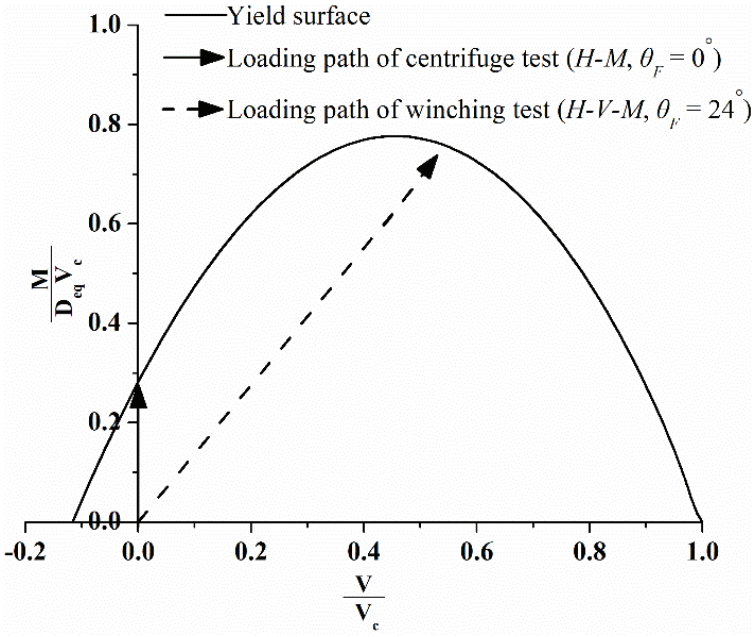

Fig. 13. Comparison of the loading path between horizontal loading (centrifuge) and field winching test

From Fig. 13 the moment capacity in a winching test is expected to be 2.64 times larger than under the conditions simulated in the centrifuge. After scaling the centrifuge-measured moment capacities by this factor, they were compared with the results of *n*=12 winching tests reported in Défossez *et al*. (2021), where the tops of the trees were removed, leaving a 3 m high stem to eliminate the contribution of the crown load, as the closest field comparators in Fig. 14, with diameter at breast height (DBH) squared multiplied by stem length (a parameter to describe the stem volume) of tested trees plotted against the corresponding moment capacity. It should be noted that the volumetric factors (DBH^2×length) were lower in these field tests compared with this study (ND = 1.32 m^3 and WS = 1.47 m^3, both at prototype scale) as the trees in the field were younger.

As a result of this difference in tree age and biomass, a further *n*=1960 in-situ winching test results conducted by Forest Research UK (Nicoll *et al.*, 2006b) and covering a

558 wider range of species, age, size and ground conditions were added to Fig. 14. A subset
559 (n=95) has been extracted for only pine species (Scots Pine, *Pinus sylvestris* and Lodge-
560 pole Pine, *Pinus contorta*) found in podzols, to be most representative of the centrifuge
561 test conditions. It should be noted that in this dataset the crowns of trees were retained,
562 the ground water table position and loading rate are unspecified and the field soils
563 (which may have different soil textures (e.g. clay) and initial densities/porosities, thus
564 different soil dilatancy behaviours and permeabilities, affecting the peak shear strength
565 and the excess pore water pressure generated under a faster loading rate and which may
566 have been subjected to cycles of wetting and drying and hence a complex stress history)
567 and root architectures may vary widely, so these data points serve as a general indica-
568 tion of comparative moment capacity. Nonetheless, the peak scaled moments (when
569 scaled to be equivalent to winching conditions) from the centrifuge tests were consistent
570 with the in-situ tests.
571

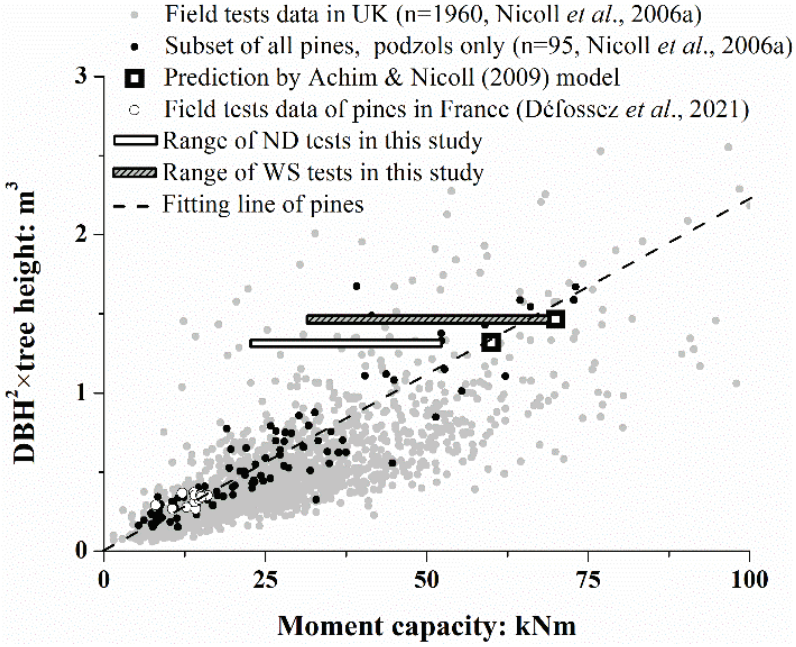

572

573 **Fig. 14. Comparison of peak moment resistance (as equivalent to trees in field winching tests)**

Insights into failure mechanisms

For fully saturated cases, parts of the windward horizontal roots in the tests were vulnerable to breakage (Fig. 7) and this was consistent with previous field observations (Coutts, 1983, 1986). Also, when trees were pushed further under faster loading, leeward laterals were observed to have been broken and clear sudden drops appeared on the moment-rotation curve beyond 40° rotation (e.g. Fig. 11c). The breakage of leeward roots is consistent with observations from field winching tests by Crook & Ennos (1996), who found that the anchorage resistance started to reduce after the leeward roots were damaged. There were no clear drops in the slower/drained saturated tests possibly indicating that the rotation angle limit of the apparatus ($\leq 30^{\circ}$) was insufficient to cause failure of leeward roots.

For lowered water table cases, all windward laterals were broken, along with breakage of part of the remaining horizontal roots, determined by the root architectures and presence (or not) of fibres. In all partially saturated tests, the taproot complex was found to have broken, potentially inducing the sharp reductions of moment resistance at around 5° and 10° rotation for ND and WS models, respectively. In some previous field testing, a large root-soil plate was formed during push-over (e.g. Coutts, 1986; Danjon *et al.*, 2005), which was not identified in this study. Using the simplified method presented in Achim & Nicoll (2009), if the shape of a root-soil plate is assumed to be a half spheroid, the minimum required moments at prototype scale to lift the root plate are approximately 60 and 70 kNm for the ND and WS models, respectively, which are at the top end of the scaled moment capacities recorded in this study (Fig. 14). It appears, therefore, that breakage of the taproot complex in the partially saturated cases limited the moment capacity of the root system before the root plate mechanism would

598 have formed. This has been observed in the field, especially on young trees with stem
599 leaning (Danquechin Dorval *et al*., 2016).
600
601 *Relationship between moment capacity, soil effective stress and failed roots*
602 Combined with the results of drained push-over tests of ND and WS models under 1***g***
603 conditions in fully saturated soil (Zhang *et al.*, 2020), the peak moment resistance of
604 trees under lateral loads under different conditions are listed in Table 6, with the effec-
605 tive confining stress of the soil at the middle depth of the root system in each case
606 calculated (using Equation (1)). As presented above, the fibrous root fraction increased
607 the moment capacity by approximately 20% (Fig. 9). With this effect removed, as
608 shown in Fig. 15, for all drained tests, a positive linear correlation was observed with
609 effective stress with a correlation coefficients $R^2 > 0.9$. Additionally, it is evident that
610 the gradient of the linear fit is significantly steeper for the WS models, meaning that
611 the overturning behaviour was more significantly affected by the effective stress (water
612 table position) for this particular root architecture.
613
614 **Table 6. Moment capacities of root systems at model scale and related soil effective stress**

Test model	Soil effective stress: kPa	***g***-level	Moment capacity: Nmm	Moment capacity removing fibre effect: Nmm
ND saturated	9.2	20	1083	1083
ND water table 1.85m	22.5		2153	2153
ND + fibres saturated	9.2		1375	1146
ND + fibres water table 1.05m	19.5		2065	1721
ND + fibres water table 1.85m	22.5		2478	2065
ND saturated (Zhang *et al*., 2020)	0.5	1	168	168
WS saturated	6.6	20	1496	1496
WS water table 1.85m	18.0		3340	3340
WS saturated (Zhang *et al*., 2020)	0.3	1	181	181

615

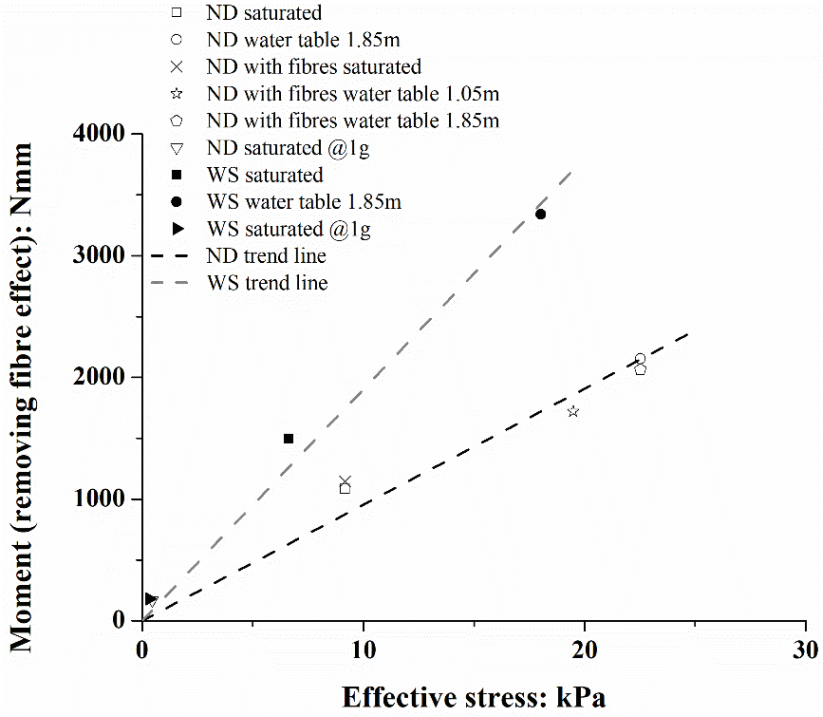

Fig. 15. Moment capacities of at model scale under different soil effective stress

The breakage of roots presented in Fig. 7 could also be correlated with the confining stress. As fibres and fast loading rate increased the moment capacity, which were approximately proportional to the effective stress (by roughly 20% and 60%, based on the average increase of moment capacity for ND and WS in comparison to drained saturated tests respectively), these effects could be approximately corrected for by considering the nominal effective stress around the roots to be 20% and 60% higher than that suggested by the depth and position of the water table. From inspection of breakages in ND models post-test, the total cross-sectional areas of broken horizontal roots in windward, leeward and side zones, broken sinker roots originating from shallow laterals, and the broken central taproot complex, are presented in Table 7. It was found that the Pearson correlation coefficient between these parameters and effective stress were 0.90,

630 0.51, 0.69, -0.10, and 0.98, respectively, indicating that the breakages of windward lat-
631 erals and the central tap root complex were positively correlated to the confining stress
632 (Fig. 16), such that these roots were principally responsible for increasing moment ca-
633 pacity when effective confining stresses were enhanced. However, this also resulted in
634 more breakages on windward horizontal roots and the taproot complex.
635

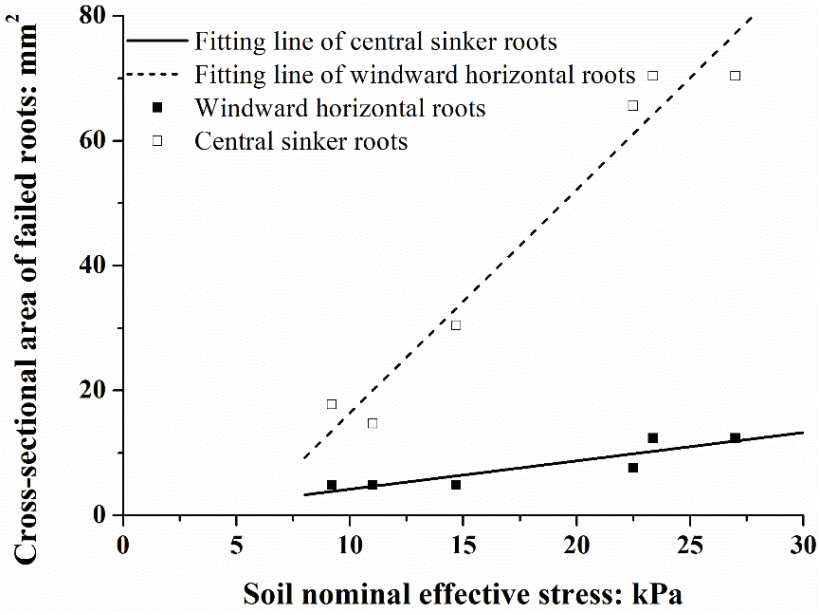

636

637 **Fig. 16. Total cross-sectional area of failed windward laterals and central sinkers of model ND**
638 **under different nominal effective stress (all values expressed at model scale)**

639 **Table 7. Total cross-sectional area of failed roots at model scale in different zones and related nominal soil effective stress at mid-depth of root system**

Test model	Nominal soil effective stress: kPa	Windward laterals: mm^2	Leeward laterals: mm^2	Side laterals: mm^2	Sinker roots: mm^2	Taproot complex: mm^2
ND saturated	9.2	4.8	0.0	0.0	3.3	17.8
ND water table 1.85m	22.5	7.5	8.2	18.4	3.3	65.5
ND + fibres saturated	11.0	4.8	0.0	0.0	5.5	14.7
ND + fibres water table 1.05m	23.4	12.4	0.0	5.5	9.7	70.4
ND + fibres water table 1.85m	27.0	12.4	4.8	7.6	5.5	70.4
ND fast loading rate	14.7	4.8	4.8	0.0	24.0	30.4

640

Implications for practice and future research

During a windstorm, often accompanied by rainfall-induced changes in soil moisture, the anchorage resistance of trees is highly likely to be lower than that measured in field winching tests conducted in good weather when soil water content is lower. This suggests that greater effort should be made to measure groundwater conditions at the time of conducting field winching tests and that test conditions should target those closest to the expected critical conditions, unless subsequent modelling will be conducted to account for any difference in groundwater.

The actual loading conditions from rock-fall impacts or wind actions are likely to apply negligible or even tensile vertical loading (in the case of wind), meaning winching tests may over-predict overturning capacity for risk assessment purposes. However, compressive vertical loading components should be taken into account for lateral loading from debris flows due to the weight of the flowing or ponded material above the root system. The higher moment capacity generated by the shallow but wider root system may be used to inform species selection when trees are to be planted to have a protective role (e.g. sacrificial planting used as a windbreak to protect commercial stands).

The results of this study also indicate that loading rate is also an important consideration in field testing or numerical simulation. Even for a soil which would typically be considered relatively insensitive to rate, such as that used in this study, a clear difference was observed when comparing test rates which were broadly representative of slow winching tests and fast environmental loading events. Finer-grained soil textures (e.g. clay) may be more sensitive to differences in loading rate as a function of their lower permeability (and therefore slower consolidation).

CONCLUSIONS

This paper has presented an investigation into the push-over behaviour of tree root systems under lateral loading using repeatably printable 1:20 scale models in centrifuge tests. Four main factors influencing the stiffness and capacity of tree root systems under lateral loading were considered, namely: (i) groundwater level (i.e. the magnitude of soil suction) (ii) root morphology (iii) finer root fraction and (iv) loading rate.

It was found that lowering the water table or increasing the loading rate increased the effective soil confining stress, which was positively correlated to the tree root system moment capacity. Despite higher moment capacity and stiffness, root-soil interaction in partially saturated soil was more brittle (compared to highly ductile behaviour in fully saturated soil), with more breakages in windward horizontal roots and the taproot complex. This strong influence of groundwater condition on strength and stiffness through the variation in load paths within the root architecture therefore suggests that it is important to measure groundwater conditions when conducting field tests if behaviour measured during such testing is to be appropriately correlated to performance under critical environmental loading conditions.

In terms of root architecture, horizontal roots along the predominant wind direction and the central taproot complex contributed most significantly to the resistance. Accounting for the finer root fraction (using fibres) enhanced the peak moment capacity by approximately 20% by reinforcing the surrounding soil for the ‘structural’ root-soil interactions. This suggests that in numerical modelling studies, simulating the largest, most structural roots will capture the majority of the response, and that these can be used to define the smallest element size (for capturing root-soil interaction) rather than the extremely fine roots, resulting in models that are more computationally-efficient. Additionally, approximately 75% of the moment capacity could be preserved by the

root systems under reloading after being pushed to a large rotation of 50°. This is important when considering debris flow or rock impact against trees on slopes as it suggests that trees that have been substantially rotated by an event, rather than suffering trunk breakage (e.g. when the ground is saturated and overturning predominates over breakage) will retain a substantial residual resistance to future events with a short return period.

The vertical confinement from a winching test appears to have a significant effect (up to 264%) on the measured moment capacity. Accounting for this resulted in a favourable comparison between centrifuge (*H-M*) and field winching tests (*V-H-M*). The actual loading conditions from rock-fall impacts or wind actions are likely to apply negligible or even tensile vertical loading (in the case of wind), meaning the centrifuge tests are more representative of these conditions and winching tests may over-predict overturning capacity for risk assessment purposes. Differences in loading rate between winching tests and dynamic events are also likely to affect the ability of a conventional winching test to represent the behaviour of a tree under environmental loading. No root-plate mechanisms were observed (even in tests with higher matric suction and potentially binding fibrous material) suggesting that new models for estimating capacity based on localised root-soil interaction (pull-out/through and breakage) would be complementary to existing root-plate-based methods.

ACKNOWLEDGEMENTS

The first author would like to acknowledge the financial support of the China Scholarship Council (CSC) and the Norman Fraser Design Trust. The third author would like to acknowledge the funding provided by the Research Grants Council of the Hong Kong

Special Administrative Region, (GRF/16202720 and CRF/C6006-20G) and the National Natural Science Foundation of China (NSFC) under the Excellent Youth Scientist Scheme (H. K. & Macau) (project no. 51922112). Frederic Danjon is gratefully acknowledged for the provision of field root architecture data. Gary Callon is also acknowledged for printing the root models used in this study, as are Mark Truswell and Grant Kydd for their assistance in conducting the centrifuge tests at the University of Dundee.

NOTATION

c' soil apparent cohesion

C_v coefficient of consolidation

D_{eq} equivalent diameter of the model root system

$d_{r,ave}$ weighted-average prototype root diameter

D_{10} particle diameter at which 10% is smaller

D_{30} particle diameter at which 30% is smaller

D_{60} particle diameter at which 60% is smaller

F measured horizontal force

$\boldsymbol{g}$ gravitational acceleration

h distance between the loading point and the top of root

H horizontal loading

L length of the line in winching test

m fitting parameter for the van Genuchten model

M toppling loading/moment resistance of the tree push-over

M_p peak moment resistance of the tree push-over

m_t mass of the tree trunk

n fitting parameter for the van Genuchten model

N $\boldsymbol{g}$-level

743 Pe Peclet number

744 R^2 correlation coefficient

745 s matric suction

746 s_e air-entry value

747 t loading time

748 u_a pore air pressure (atmospheric)

749 u_w pore water pressure

750 v maximum rate of shearing

751 V vertical loading

752 V_c vertical compressive (bearing) capacity of a shallow foundation

753 V_t vertical tensile (uplift) capacity of a shallow foundation

754 v_H loading rate

755 α fitting parameters for the van Genuchten model

756 β empirical parameter in macroelement model

757 η empirical parameter in macroelement model

758 θ rotation of the tree trunk

759 θ_F inclination angle of the force relative to horizontal

760 θ_p rotation at peak moment

761 θ_r residual soil water content

762 θ_s saturated soil water content

763 θ_w soil water content

764 μ empirical parameter in macroelement model

765 ξ normalised vertical load in macroelement model

766 σ soil total normal stress

767 τ soil shear strength

768 ϕ' soil friction angle

769 χ effective stress parameter

770 ψ soil matric suction

771

772

773 REFERENCES

774 Achim, A. & Nicoll, B. C. (2009). Modelling the anchorage of shallow-rooted trees. *Forestry* **82**, No.
775 3, 273–284, 10.1093/forestry/cpp004.
776 British Standards Institution (1990) Methods of test for soils for civil engineering purposes - part 1:
777 General requirements and sample preparation.
778 Coutts, M. P. (1986). Components of tree stability in sitka spruce on peaty gley soil. *Forestry* **59**, No.
779 2, 173–197, https://doi.org/10.1093/forestry/59.2.173.
780 Coutts, M. P. (1983). Root architecture and tree stability. *Plant and Soil* **71**, 171–188,
781 https://doi.org/10.1007/BF02182653.
782 Coutts, M. P., Nielsen, C. C. N. & Nicoll, B. C. (1999). The development of symmetry, rigidity and
783 anchorage in the structural root system of conifers. *Plant and Soil* **217**, No. 1–2, 1–15,
784 https://doi.org/10.1023/A:1004578032481.
785 Crook, M. J. & Ennos, A. R. (1996). The anchorage mechanics of deep rooted larch, Larix europea × L.
786 japonica. *Journal of Experimental Botany* **47**, No. 10, 1509–1517,
787 https://doi.org/10.1093/jxb/47.10.1509.
788 Crook, M. J. & Ennos, A. R. (1998). The increase in anchorage with tree size of the tropical tap rooted
789 tree Mallotus wrayi, King (Euphorbiaceae). *Annals of Botany* **82**, No. 3, 291–296,
790 https://doi.org/10.1006/anbo.1998.0678.
791 Cui, P., Lin, Y.M. & Chen, C. (2012). Destruction of vegetation due to geo-hazards and its
792 environmental impacts in the Wenchuan earthquake areas. *Ecological Engineering* **44**, 61–69,
793 https://doi.org/10.1016/j.ecoleng.2012.03.012.
794 Danjon, F., Barker, D. H., Drexhage, M. & Stokes, A. (2008). Using three-dimensional plant root
795 architecture in models of shallow-slope stability. *Annals of Botany* **101**, No. 8, 1281–1293,
796 https://doi.org/10.1093/aob/mcm199.
797 Danjon, F., Caplan, J. S., Fortin, M. & Meredieu, C. (2013). Descendant root volume varies as a
798 function of root type: estimation of root biomass lost during uprooting in Pinus pinaster.
799 *Frontiers in Plant Science* **4**, 1–16, https://doi.org/10.3389/fpls.2013.00402.
800 Danjon, F., Fourcaud, T. & Bert, D. (2005). Root architecture and wind-firmness of mature Pinus
801 pinaster. *New Phytologist* **168**, No. 2, 387–400, https://doi.org/10.1111/j.1469-
802 8137.2005.01497.x.

803 Danjon, F. & Reubens, B. (2008). Assessing and analyzing 3D architecture of woody root systems, a
804 review of methods and applications in tree and soil stability, resource acquisition and allocation.
805 *Plant and Soil* **303**, No. 1–2, 1–34, https://doi.org/10.1007/s11104-007-9470-7.
806 Danquechin Dorval, A., Meredieu, C. & Danjon, F. (2016). Anchorage failure of young trees in sandy
807 soils is prevented by a rigid central part of the root system with various designs. *Annals of Botany*
808 **118**, No. 4, 747–762, https://doi.org/10.1093/aob/mcw098.
809 Dattola, G., Ciantia, M.O., Galli, A., Blyth, L., Zhang, X., Knappett, J.A., Castellanza, R., Sala, C. &
810 Leung, A.K. (2020). A Macroelement Approach for the Stability Assessment of Trees. In
811 *National Conference of the Researchers of Geotechnical Engineering*, pp. 417-426,
812 https://doi.org/10.1007/978-3- 030-21359-6_44.
813 Défossez, P., Veylon, G., Yang, M., Bonnefond, J.M., Garrigou, D., Trichet, P. & Danjon, F. (2021).
814 Impact of soil water content on the overturning resistance of young Pinus Pinaster in sandy soil.
815 *Forest Ecology and Management* **480**, https://doi.org/10.1016/j.foreco.2020.118614.
816 Dekker, M. M., Haarsma, R. J., Vries, H. de, Baatsen, M. & van Delden, A. J. (2018). Characteristics
817 and development of European cyclones with tropical origin in reanalysis data. *Climate Dynamics*
818 **50**, No. 1–2, 445–455, https://doi.org/10.1007/s00382-017-3619-8.
819 Dupont, S. & Brunet, Y. (2008). Impact of forest edge shape on tree stability: A large-eddy simulation
820 study. *Forestry* **81**, No. 3, 299–315, https://doi.org/10.1093/forestry/cpn006.
821 Finnie, I. M. S. & Randolph, M. F. (1994) Punch-through and liquefaction induced failure of shallow
822 foundations on calcareous sedi- ments. In *Seventh Int ConfBehav Offshore Struct*, No 1, 217–230.
823 Gandhi, K. J. K., Gilmore, D. W., Katovich, S. A., Mattson, W. J., Zasada, J. C. & Seybold, S. J.
824 (2008). Catastrophic windstorm and fuel-reduction treatments alter ground beetle (Coleoptera:
825 Carabidae) assemblages in a North American sub-boreal forest. *Forest Ecology and Management*
826 **256**, No. 5, https://doi.org/1104–1123, 10.1016/j.foreco.2008.06.011.
827 Gardiner, B. A. & Quine, C. P. (2000). Management of forests to reduce the risk of abiotic damage - A
828 review with particular reference to the effects of strong winds. *Forest Ecology and Management*
829 **135**, No. 1–3, 261–277, https://doi.org/10.1016/S0378-1127(00)00285-1.
830 Harnas, F. R., Rahardjo, H., Leong, E. C., Tan, P. Y. & Ow, L. F. (2016). Stability of containerized
831 urban street trees. *Landscape and Ecological Engineering* **12**, No. 1, 13–24,
832 https://doi.org/10.1007/s11355-015-0272-4.

833 Jakob, M. & Lambert, S. (2009). Climate change effects on landslides along the southwest coast of
834 British Columbia. *Geomorphology* **107**, No. 3–4, 275–284,
835 https://doi.org/10.1016/j.geomorph.2008.12.009.
836 Kamchoom, V., Leung, A. K. & Ng, C. W. W. (2014). Effects of root geometry and transpiration on
837 pull-out resistance. *Geotechnique Letters* **4**, No. 4, 330–336,
838 https://doi.org/10.1680/geolett.14.00086.
839 Khalili, N. & Khabbaz, M. H. (1998). A unique relationship for χ for the determination of the shear
840 strength of unsaturated soils. *Geotechnique* **48**, No. 5, 681–687,
841 https://doi.org/10.1680/geot.1998.48.5.681.
842 Kim, Y., Rahardjo, H. & Tsen-Tieng, D. L. (2020). Stability analysis of laterally loaded trees based on
843 tree-root-soil interaction. *Urban Forestry & Urban Greening* **49**, 126639,
844 https://doi.org/10.1016/j.ufug.2020.126639.
845 Lateltin, O., Haemmig, C., Raetzo, H. & Bonnard, C. (2005). Landslide risk management in
846 Switzerland. *Landslides* **2**, No. 4, 313–320, https://doi.org/10.1007/s10346-005-0018-8.
847 Liang, T., Bengough, A. G., Knappett, J. A., MuirWood, D., Loades, K. W., Hallett, P. D., Boldrin, D.,
848 Leung, A. K. & Meijer, G. J. (2017). Scaling of the reinforcement of soil slopes by living plants
849 in a geotechnical centrifuge. *Ecological Engineering* **109**, 207–227,
850 https://doi.org/10.1016/j.ecoleng.2017.06.067.
851 Liang, T., Knappett, J. A. & Duckett, N. (2015). Modelling the seismic performance of rooted slopes
852 from individual root–soil interaction to global slope behaviour. *Géotechnique* **65**, No. 12, 995–
853 1009, https://doi.org/10.1680/jgeot.14.P.207.
854 Liang, T., Knappett, J.A., Leung, A. Carnaghan, A., Bengough, A.G. & Zhao, R. (2020). A critical
855 evaluation of predictive models for rooted soil strength with application to predicting the seismic
856 deformation of rooted slopes. Landslides **17**, No. 1, 93–109. https://doi.org/10.1007/s10346-019-
857 01259-8
858 McCarthy, J. K., Hood, I. A., Brockerhoff, E. G., Carlson, C. A., Pawson, S. M., Forward, M., Walbert,
859 K. & Gardner, J. F. (2010). Predicting sapstain and degrade in fallen trees following storm
860 damage in a Pinus radiata forest. *Forest Ecology and Management* **260**, No. 9, 1456–1466,
861 https://doi.org/10.1016/j.foreco.2010.07.044.
862 Meijer, G. J., Bengough, A. G., Knappett, J. A., Loades, K. W. & Nicoll, B. C. (2018). In situ

measurement of root reinforcement using corkscrew extraction method. *Canadian Geotechnical Journal* **55**, No. 10, 1372–1390, https://doi.org/10.1139/cgj-2017-0344.

Meijer, G. J., Knappett, J. A., Nicoll, B. C., Loades, K. W. & Bengough, A. G. (2015). New in situ techniques for measuring the properties of root-reinforced soil – laboratory evaluation. *Géotechnique* **66**, No. 1, 27–40, https://doi.org/10.1680/jgeot.15.p.060.

Meijer, G. J., Wood, D. M., Knappett, J. A., Bengough, A. G. & Liang, T. (2019). Root branching affects the mobilisation of root-reinforcement in direct shear. In *E3S Web of Conferences* **92**, 12010, https://doi.org/10.1051/e3sconf/20199212010.

Mickovski, S. B., Bengough, A. G., Bransby, M. F., Davies, M. C. R., Hallett, P. D. & Sonnenberg, R. (2007). Material stiffness, branching pattern and soil matric potential affect the pullout resistance of model root systems. *European Journal of Soil Science* **58**, No. 6, 1471–1481, https://doi.org/10.1111/j.1365-2389.2007.00953.x.

Mickovski, S. B., Bransby, M. F., Bengough, A. G., Davies, M. C. R. & Hallett, P.D. (2010). Resistance of simple plant root systems to uplift loads. *Canadian Geotechnical Journal* **47**, No. 1, 78–95, https://doi.org/10.1139/T09-076.

Mickovski, S. B. & Ennos, A. R. (2003). Model and whole-plant studies on the anchorage capabilities of bulbs. *Plant and Soil* **255**, No. 2, 641–652, https://doi.org/10.1023/A:1026007229517.

Moore, J. R., Tombleson, J. D., Turner, J. A. & Van Der Colff, M. (2008). Wind effects on juvenile trees: A review with special reference to toppling of radiata pine growing in New Zealand. *Forestry* **81**, No. 3, 377–387, https://doi.org/10.1093/forestry/cpn023.

Nakahara, T., Iai, S. & Tobita, T. (2005). Generalised scaling relations for dynamic centrifuge tests. *Géotechnique* **55**, No. 5, 355–362, https://doi.org/10.1680/geot.2005.55.5.355.

Nelson, O., Kassim, A., Yunusa, G. H. & Talib, Z. A. (2015). Modelling the effect of wind forces on landslide occurrence in Bududa district, Uganda. *Jurnal Teknologi* **77**, No. 11, 35–42, https://doi.org/10.11113/jt.v77.6392.

Nicoll, B.C., Gardiner, B.A., Rayner, B. & Peace, A.J. (2006a). Anchorage of coniferous trees in relation to species, soil type, and rooting depth. *Canadian Journal of Forest Research* **36**, No. 7, https://doi.org/1871–1883, 10.1139/X06-072.

Nicoll, B.C., Berthier, S., Achim, A., Gouskou, K., Danjon, F. & Van Beek, L.P.H. (2006b). The architecture of Picea sitchensis structural root systems on horizontal and sloping terrain. *Trees*

20, No. 6, 701–712, https://doi.org/10.1007/s00468-006-0085-z.

Nicoll, B.C., Gardiner, B.A. & Peace, A.J. (2008). Improvements in anchorage provided by the acclimation of forest trees to wind stress. *Forestry* **81**, No. 3, 389–398, https://doi.org/10.1093/forestry/cpn021.

Rahardjo, H., Harnas, F. R., Leong, E. C., Tan, P. Y., Fong, Y. K. & Sim, E. K. (2009). Tree stability in an improved soil to withstand wind loading. *Urban Forestry & Urban Greening* **8**, No. 4, 237-247, https://doi:10.1016/j.ufug.2009.07.001

Ramos-Rivera, J., Rahardjo, H., Tsen-Tieng, D. L., Xuefeng, N. & King, F. Y. (2020). Mechanical response of the real tree root architecture under lateral load. *Canadian Journal of Forest Research* **50**, No. 7, 595-607, https://doi.org/10.1139/cjfr-2019-0332

Schelhaas, M.J., Hengeveld, G., Moriondo, M., Reinds, G.J., Kundzewicz, Z.W., ter Maat, H. & Bindi, M. (2010). Assessing risk and adaptation options to fires and windstorms in European forestry. *Mitigation and Adaptation Strategies for Global Change* **15**, No. 7, https://doi.org/681–701, 10.1007/s11027-010-9243-0.

Schmidlin, T.W. (2009). Human fatalities from wind-related tree failures in the United States, 1995-2007. *Natural Hazards* **50**, No. 1, 13–25, https://doi.org/10.1007/s11069-008-9314-7.

Schwarz, M., Cohen, D. & Or, D. (2011). Pullout tests of root analogs and natural root bundles in soil: Experiments and modeling. *Journal of Geophysical Research: Earth Surface* **116**, No. 2, 1–14, https://doi.org/10.1029/2010JF001753.

Stokes, A. (1999). Strain distribution during anchorage failure of Pinus pinaster Ait. at different ages and tree growth response to wind-induced root movement. *Plant and Soil* **217**, No. 1–2, 17–27, https://doi.org/10.1007/978-94-017-3469-1_2.

Stone, K. J. L. & Wood, D. M. (1992) Effects ofdilatancy and particle size observed in model tests on sand. *Soils Found* **32**, 43–57.

Van Genuchten, M. (1980). A closed-form equation for predicting the hydraulic conductivity of unsaturated soils. Soil Sci. Soc. Am. J. 44, No. 5, 892–898.

Wang, K. & Brennan, A.J. (2015). Centrifuge Modelling of Fibre-Reinforcement as a Liquefaction. In *6th International Conference on Earthquake Geotechnical Engineering*, Christchurch, New Zealand.

Wood, D. M. (2004). *Geotechnical modelling*. Spon Press, Abingdon.

923 Yang, M., Défossez, P., Danjon, F., Dupont, S. & Fourcaud, T. (2017). Which root architectural
924 elements contribute the best to anchorage of Pinus species? Insights from in silico experiments.
925 *Plant and soil* **411**, No. 1-2, 275-291, https://doi.org/10.1007/s11104-016-2992-0
926 Zhang, X., Knappett, J. A., Leung, A. K., Ciantia, M. O., Liang, T. & Danjon, F. (2020). Small-scale
927 modelling of root-soil interaction of trees under lateral loads. *Plant and Soil* **456**, No. 1–2, 289–
928 305, https://doi.org/10.1007/s11104-020-04636-8.
929 Zhang, X., Knappett, J. A., Leung, A. K. & Liang, T. (2018). Physical modelling of soil-structure
930 interaction of tree root systems under lateral loads. In *Physical Modelling in Geotechnics*, CRC
931 Press, London, No. 1, pp. 481-486, https://doi.org/10.1201/9780429438646.